



HAL
open science

Using FBGS to estimate the horizontal response of a monopile in a geotechnical centrifuge

Zhong-Sen Li, Matthieu Blanc, Luc Thorel

► **To cite this version:**

Zhong-Sen Li, Matthieu Blanc, Luc Thorel. Using FBGS to estimate the horizontal response of a monopile in a geotechnical centrifuge. *International Journal of Physical Modelling in Geotechnics*, 2020, 20 (3), pp.164-174. 10.1680/jphmg.19.00022 . hal-02516732

HAL Id: hal-02516732

<https://hal.science/hal-02516732>

Submitted on 5 May 2021

HAL is a multi-disciplinary open access archive for the deposit and dissemination of scientific research documents, whether they are published or not. The documents may come from teaching and research institutions in France or abroad, or from public or private research centers.

L'archive ouverte pluridisciplinaire **HAL**, est destinée au dépôt et à la diffusion de documents scientifiques de niveau recherche, publiés ou non, émanant des établissements d'enseignement et de recherche français ou étrangers, des laboratoires publics ou privés.

This is an electronic reprint of the original article.
This reprint may differ from the original in pagination and typographic detail.

Li, Zhongsen; Blanc, Matthieu; Thorel, Luc

Using FBGS to estimate the horizontal response of a monopile in a geotechnical centrifuge

Published in:
International Journal of Physical Modelling in Geotechnics

DOI:
[10.1680/jphmg.19.00022](https://doi.org/10.1680/jphmg.19.00022)

Published: 01/05/2020

Document Version
Peer reviewed version

Please cite the original version:
Li, Z., Blanc, M., & Thorel, L. (2020). Using FBGS to estimate the horizontal response of a monopile in a geotechnical centrifuge. *International Journal of Physical Modelling in Geotechnics*, 20(3), 164-174. [1900022]. <https://doi.org/10.1680/jphmg.19.00022>

This material is protected by copyright and other intellectual property rights, and duplication or sale of all or part of any of the repository collections is not permitted, except that material may be duplicated by you for your research use or educational purposes in electronic or print form. You must obtain permission for any other use. Electronic or print copies may not be offered, whether for sale or otherwise to anyone who is not an authorised user.

Using Fibre Bragg Grating sensors to estimate the horizontal response of a monopile in geotechnical centrifuge

Zhong-Sen Li, post-doctor^{1,2}; Matthieu Blanc, researcher^{1*}; Luc Thorel, senior researcher¹

¹ Laboratory of Geomaterials and Modelling in Geotechnics, Department GERS, IFSTTAR, Route de Bouaye, Bouguenais 44344, France

² Department of Civil Engineering, Aalto University, Otaniemi 02150, Finland

* Corresponding author: matthieu.blanc@ifsttar.fr, +33 2 40 84 58 18

Abstract: A 50-mm-diameter circular aluminium tube was instrumented with two optical fibres that consist of 13 Fibre Bragg Grating sensors (FBGS) for each. The performance of the FBGS was evaluated by applying a series of increasing transversal loads at 1×g level and comparing the strains measured by FBGS with those calculated from the Euler-Bernoulli beam theory. Centrifuge test was then conducted at 100×g to estimate the transversal response of the calibrated model pile that had been jacked 450 mm into saturated sand and horizontally loaded at 500 mm above the ground. The profiles of the normal strain, bending moment, soil reaction and pile deflection were measured or determined, allowing to construct the soil reaction – pile deflection (P-y) curves. The results confirmed the reliability of the FBGS at 100×g by giving satisfactory measurements on bending moments and coherent measurements on shear force at the ground level.

Key words: Centrifuge; Monopile; Transversal loading; Fibre Bragg Grating sensors; Sand

Manuscript revised: 2019-11-01

Number of words: 3746

Number of Table: 2

Number of Figure: 8

List of notation

P	soil reaction (kN/m)
y	pile deflection (mm)
ε	normal strain of the pile
λ	peak wavelength of the fibre Bragg grating (nm)
$\Delta\lambda$	peak wavelength shift (nm)
k	gage factor of the optical fibre
E	Young modulus (GPa)
I	moment of inertia of an area (m ⁴ or mm ⁴)
F	applied vertical weight during pile calibration (N)
D	external diameter (mm)
d	inner diameter (mm)
M	bending moment (N.m)
L	Embedded pile length (m)
l	lever arm (mm)
L	embedded pile length (m)
H	applied horizontal force at the pile head (N)
V	shear force (N)
g	gravitational acceleration (m/s ²)
$d_{10}/d_{50}/d_{60}$	diameter at which 10, 50 or 60% of the sample's mass is comprised of smaller particles (μm)
ρ_{d-min}	minimum dry density (g/cm ³)
ρ_{d-max}	maximum dry density (g/cm ³)
A	distance between two adjacent fringe (nm)
n	positive integer
z	depth of the pile embedment (mm)
C_u	coefficient of uniformity

1 **1. Introduction**

2 Monopile is a typical foundation for offshore wind farms. It takes over 80% of recently installed wind
3 turbines (Wind Europe, 2017) and represent about 15-20% of the total investment. The lifecycle of
4 the monopile is influenced by the horizontal service loads resulting from winds, currents and waves.
5 The generation of horizontal deflection may degrade the foundation soil and as a result trigger the
6 instability problems. Faced with the increasing capacity of the next-generation wind turbines, the
7 dimension of the future monopiles is expected to increase, for example, to as large as 10 m in
8 diameter. For such large-diameter monopiles, current design codes for long and slender piles are
9 deemed inappropriate and new standards need to be developed.

10 In the literature, three experimental methods exist to characterise the response of pile or monopile
11 under transversal loads: i) the full-scale field tests (e.g. Davisson and Salley, 1969; Baguelin et
12 Jézéquel, 1972, Cox et al., 1974; Reese et al., 1974; Ting, 1987; Little and Briaud, 1988; Koukoura
13 et al., 2015; Barbosa et al., 2017; Jardine et al., 2018; McAdam et al., 2018); ii) reduced-scale
14 laboratory tests (e.g. LeBlanc et al., 2010; Abadie et al., 2018) and iii) reduced-scale centrifuge tests
15 (e.g. Georgiadis et al., 1992; Verdure et al., 2003; Rosquoet et al., 2007; Li et al., 2010; Klinkvort
16 and Hededal, 2013, 2014; Klinkvort et al., 2013, 2019; Choo and Kim, 2015; Truong et al., 2018).
17 Each above-mentioned method presents its own inherent advantages and disadvantages. For
18 performing parametric studies in a first step, reduced-scale laboratory and centrifuge tests are more
19 feasible due to the consideration of testing budget. Comparing to laboratory tests, centrifuge tests at
20 elevated gravity have the advantage of reproducing the field stress condition for monopiles. Through
21 carrying out centrifuge tests, researchers were able to test monopiles as large as 50 mm in diameter
22 (e.g. Li et al, 2010, Klinkvort et al., 2019). The pile local strains were measured and then used to
23 determine the soil reaction – pile deflection (P-y) relationship. These results, together with the full-

24 scale field tests and reduced-scale laboratory tests, are of interest for the design of next generation
25 monopiles.

26 The present study is part of the SOLCYP+ project (France Energies Marines, 2017), which is an
27 extension of the SOLCYP project (Puech and Garnier, 2017). The main objective was to
28 experimentally investigate the response of the model piles under horizontal load in geotechnical
29 centrifuge and then to extrapolate the prototype pile behaviour. Fibre Bragg Grating sensors (FBGS)
30 were used to measure the local strains and to determine the moment profile of the pile. Experimental
31 results are presented following the local pile analysis (Garnier, 2013).

32 **2. Principle and geotechnical application of FBGS**

33 Exposing the Germanium-doped optical fibre to the spatial pattern of ultraviolet light (e.g. Hill and
34 Meltz, 1997; Kreuzer, 2006) can artificially alter the refractive index of the fibre and form a periodic
35 modulation of the refractive index (i.e., grating). When a beam of light passes a grating, part of the
36 light will be reflected and the other be transmitted. The reflected lights accumulate and form a peak
37 if an integer of the light wavelength fits into two times of the fringe spacing, as shown in Figure 1.

38 Under the effect of the external stress or temperature, the optical fibre shrinks or swells. This
39 shrinkage-swelling results in a change in grating period and as a result a corresponding shift of the
40 reflected peak wavelength in the recorded spectra. Under temperature-controlled condition, the strain
41 (ε) can be calculated with the peak wavelength shift ($\Delta\lambda$) by the following formula:

$$42 \quad \varepsilon = \frac{\Delta\lambda}{\lambda k} \quad (1)$$

43 where λ (nm) is the initial peak wavelength under null external stress (i.e., reference scan), $\Delta\lambda$ (nm)
44 is the peak wavelength shift and k, the gage factor, is equal to 0.78 for the fibre used in this study.

45 As the FBGS has very small dimension (e.g., diameter of several hundred micro-meters), it can be
46 adhered on or embedded into the piles or beams without significantly changing their geometry and
47 mechanical property. For such reason, it has been increasingly used. In geotechnical laboratory and
48 field testing, FBGS have been used to measure the load transfer of the model pile (e.g., Lee et al.,
49 2004), the strain distribution along the soil nails during pull-out test (e.g., Zhu et al., 2007, 2011;
50 Hong et al., 2017) and the transversal displacement of ballast under cyclic loading conditions (e.g.,
51 Hussaini et al., 2015). Besides, FBGS have been used to monitor the dynamic process of the wind
52 turbine blades (e.g., Park et al., 2011), large pile under vertical driving conditions (e.g., Doherty et
53 al., 2015) and strains of buried pipelines under different external loads (e.g. Glisic and Yao, 2012;
54 Simpson et al., 2015; Ni et al., 2018).

55 However, the report of the FBGS in geotechnical centrifuge is limited. Kapogianni et al. (2010)
56 investigated the performance of FBGS in a drum centrifuge at ETH Zurich. The FBGS gave coherent
57 measurements at different g-level (0-100 g) even though the unstable measuring signal was observed
58 due to the movements of the FBGS cables. Da Silva et al. (2016) reported their experience on FBGS
59 instrumentation and calibration in centrifuge test at the University of Cambridge. A first issue that
60 they considered was the location and orientation of the fibre optic interrogator. In their study, the
61 interrogator was placed on the centrifuge beam as close as possible to the centre to minimise the
62 gravitational acceleration experienced by the interrogator. In addition, the interrogator box was
63 orientated such that the axis of the fans aligned with the direction of the gravitational acceleration to
64 minimise impact of g-level on the operation of the interrogator. After these efforts, the authors found
65 that the interrogator remained securely in place with g-level up to 40 g (i.e., 6 g for the interrogator).
66 Excellent correlation was achieved between the strains measured by FBGS and those by LVDT, with
67 the difference generally smaller than 5%. To avoid the high g-forces within the interrogator, Correia
68 et al. (2016) reported a new method to place the FBGS interrogator. This method consists of using a

69 fibre optic rotary joint and placing the interrogator outside of the centrifuge. At Chang'an University
70 (China), Weng et al. (2016) conducted a series of centrifuge tests, using both FBGS and strain gauge
71 to measure the vertical strains of a jacked steel pile previously soaked by water. The difference
72 between the strains measured by FBGS and the strains measured by strain gauges was, in most cases,
73 within 10%.

74 In conclusion, the FBGS i) provides a precise, reliable and convenient method to monitor strain
75 change of piles and pipes; ii) allows multiple strain measurements with a single fibre; iii) is easy to
76 be installed and suitable under both static and dynamic load conditions and iv) is rarely used in
77 geotechnical centrifuge. Compared to the strain measuring methods that the authors previously
78 adopted (e.g., gluing the strain gages outside or even inside the tube in Rosquoët et al., 2007 and El
79 Haffar et al., 2019), the choice of the optical fibres in this study was mainly to maintain the wall
80 thickness of the tube while working on an open-ended model pile.

81 **3. Instrumentation and calibration of the model pile**

82 The geometric and mechanical characteristics of the model pile are described in Figure 2 and Table
83 1. The choice of an aluminium tube instead of a steel bar allows to respect the key scale factor of the
84 rigidity (EI) while maintaining a suitable tube thickness for embedding FBG sensors. Besides,
85 aluminium has been commonly used in geotechnical centrifuge to reproduce the behaviour of steel
86 structures (e.g. Ng et al., 2015; Saiyar et al., 2016). The pile was chiselled with two semi-cylindrical
87 grooves that are diametrically opposed. The radius of the grooves is 0.5 mm, i.e., 1/5 the wall
88 thickness of the pile. Two 200-micrometer-diameter optical fibres were laid straight in the grooves
89 and then sealed by a bi component cold curing epoxy, i.e., X120 adhesive. X120 adhesive was chosen
90 mainly due to its easy usage and good strain transfer property (HBM, 2019b). Another consideration
91 was that the stiffness of the adhesiveness is smaller than that of the pile so that the local gauge

92 hardening effect can be avoided. Placing two optical fibres in an extension-compression
93 configuration, i.e., diametrically opposed as shown in Figure 2a, aimed to compensate the temperature
94 effect on the measurement. This effect can be compensated by averaging the difference of the two
95 measured strains (i.e., $\varepsilon_{av.} = (\varepsilon_{ext.} - \varepsilon_{comp.})/2$) as a temperature change has identical effect on both fibres
96 in terms of the peak wavelength shift, e.g., one fibre being compressed and features a negative strain,
97 whereas the other being stretched and has a positive strain. Within each optical fibre, 13 FBGS were
98 integrated and distributed every 25 mm for the first eight FBGS (#1 - #8) and every 50 mm for the
99 rest (#9 - #13). Such a configuration allows to measure the pile strains at 13 different positions ranging
100 from 0 - 425 mm away from the FBGS #1, as shown in Figures 2 and 3.

101 The calibration of the model pile is intended to compare the the strain measured by FBGS and that
102 calculated from the Euler-Bernoulli beam theory. Two calibrating methods are proposed: i) the pile
103 clamped at one end (i.e., cantilever beam) and ii) the pile put on two rigid supports (e.g., simply
104 supported beam). The apparatus and the corresponding schematic drawing are presented in Figure 3.
105 To avoid the possible damage on the pile end in particular for the cantilever beam configuration where
106 the pile was clamped only 10 mm at the end, the maximum applied weight F was limited, for example
107 100 N and 500 N for the cantilever and simply supported beam, respectively. For this reason, the
108 calibration strains were within 350 microstrain (10^{-6}), which cannot cover the full range of the
109 following centrifuge tests. Transversal loads were applied at $1\times g$ level with an incremental ratio of
110 about 2, i.e., 20, 50, 100 N for the cantilever beam and 20, 50, 100, 200 and 500 N for the simply
111 supported beam. In order to evaluate the performance of the FBGS under both tensile and
112 compressive conditions, the pile was calibrated at 0° (initial position) and 180° (turning the pile over).
113 As the transversal load increases, the model pile deflects and generates tensile or compressive strains.
114 These strains can be on the one hand calculated based on the direct measurements of the FBGS as

115 shown in Equation 1, and on the other hand determined by the Euler-Bernoulli beam theory using the
116 following formula:

$$117 \quad \varepsilon = \frac{MD}{2EI} \quad (2)$$

118 where M is the moment at different sections, F , the applied transversal force, D , the outside diameter
119 of the pile, E , the Young modulus of the pile and I , the moment of inertia of the section..

120 For the cantilever beam configuration, the moment M is:

$$121 \quad M = F \cdot (500 + z_{FBGS}) \quad (3)$$

122 and for the simply supported beam, the moment M is:

$$123 \quad M = \frac{F \cdot 215 \cdot (440 - z_{FBGS})}{955} \quad (4)$$

124 where z_{FBGS} is the position of the FBGS in mm, as illustrated in Figure 3.

125 Figure 4 presents the calibration results of the model pile. When the pile is clamped on one tip (i.e.,
126 cantilever beam), the transversal loads applied on the other tip generate bending moment, shear force
127 and normal stress at the cross-section of the pile. On the upper side of the neutral axis, the normal
128 stresses and strains are tensile, and on the lower side, they are compressive. The strains measured by
129 the two optical fibres (A and B) are presented in the first and second diagrams of Figure 4a, which
130 correspond to the pile at the initial position and turned 180° over, respectively. For the applied loads,
131 most experimental results (i.e., points) situate on or are very close to the correlation lines according
132 to the Euler-Bernoulli beam theory, i.e., Equation 2. Exceptions are the measurements by the FBGS
133 #13, as shown in Figure 4a. The strains measured by FBGS #13 deviate the theoretical values and the
134 difference becomes more pronounced at larger load levels (e.g., 100 N). The main reason for such
135 inaccurate measurements is that the FBGS #13 is too close (i.e., 15 mm) to the clamp, where shear

136 strains are more significant. In such case, both the Saint Venant principle and the Euler-Bernoulli
137 beam assumptions are not satisfied. The relative difference of the strain measured by FBGS (ϵ_{FBGS})
138 and that determined by Euler-Bernoulli beam theory (ϵ_{E-B}) ranges from -4.74 to 3.46% for optical
139 fibre A at initial and 180° turn-over positions if the FBGS #13 is not taken into account. Taking the
140 average value of the four measured strains (i.e., fibre A at 0° and 180°, and fibre B at 0° and 180°),
141 the bending moments are calculated with Equation 2 and then compared with the theoretical
142 correlation lines, as shown in the third diagram in Figure 4a. Apart from the last point by FBGS #13,
143 the experimental points are in very good agreement with the theoretical prediction.

144 When the pile is supported by two tips (i.e., simply supported beam) and the transversal loads are
145 applied in between, strains are in tension on the lower side and in compression on the upper side.
146 Similarly, the experimental points, excluding those measured by FBGS #13, are located around the
147 correlation lines (Figure 4b). However, for the maximum transversal load, the measured strains are
148 deviated from those calculated according to Euler-Bernoulli beam theory. The FBGS measurements
149 deviate from -11.99 to 4.89% from the theoretical predictions for FBGS #1-8. The relative difference
150 increases significantly for FBGS #9-13. This may result from many aspects in such a free system
151 where both the stress concentration and pile movement are possible. As concerning the moment
152 profiles, results in the third diagram of Figure 4b shows better accordance between the experiment
153 and theoretic correlations, with their difference generally smaller than 5%.

154 **4. Pile behaviour under transversal loads in centrifuge test**

155 ***4.1 Preparation of the centrifuge test***

156 The experimental study was carried out at the IFSTTAR large beam centrifuge ($D = 11 \text{ m}$)
157 inaugurated in 1985 (Corté and Garnier, 1986). The centrifuge can generate a maximum gravitational
158 acceleration of 100 g in the bracket for a sample mass up to 2 tons. The FS22DI Industrial

159 BraggMETER Interrogator box from HBM was placed in the data acquisition chamber that is attached
160 to the rotation centre. The longitude direction of the interrogator was in line with the centrifuge arm.
161 The gravitational acceleration experienced by the interrogator is estimated about 1/15 of the
162 centrifuge basket. The wavelengths of the 13 FBGS at reference scan range from 1520-1580 nm and
163 increase every 5 mm. To prepare for the centrifuge test, three steps were employed: i) model sand
164 preparation, ii) pile installation and iii) load application.

165 The model soil was the Fontainebleau NE34 poorly graded sand (Table 2). Using the automated
166 raining technique (Garnier 2001), the sand was dropped from a constant height (70 cm in this study)
167 and then pluviated into a 1200 mm (length) by 800 mm (width) by 720 mm (height) rectangular
168 strongbox. The depth of the sand mass was 560 mm and the relative density was 81%. To simulate
169 the prototype condition where the foundation is under water, the sand was saturated by slowly (about
170 6 hours) injecting water through four draining channels located at the bottom of the strongbox. The
171 attained water table was about 30 mm above the sand surface. The effective volumetric weight of the
172 saturated sand was 10.3 kN/m³.

173 Concerning the pile installation, the instrumented model pile (Figure 2) was pushed into the sand at
174 1×g level by a hydraulic jack. The jacking speed was 1 mm/s and the attained depth is 450 mm, i.e.,
175 9D. The sand level inside the pile was checked and there was no plug generated. After pile installation,
176 an electric actuator was mounted on two supporting beams that perpendicularly placed on the
177 longitudinal edges of the strongbox. The actuator has a stroke of 150 mm and can measure the load
178 with a precision of 0.1 N for a range from 0 - 5 kN. At the end of the piston, a force transducer and
179 a loading fork were integrated, aiming to measure and control the applied horizontal load. In front of
180 the actuator, a laser displacement transducer, with measuring range of 120 mm and resolution of 20
181 μm, was fixed on a supporting beam. This allows to monitor the pile deflection at 410 mm above the
182 ground level. The established experimental set-up is schematically shown in Figure 5.

183 Centrifuge test was performed at $100\times g$ level. Horizontal load was applied through the centre of the
184 cross section by pushing the steel rod that crosses the monopile perpendicularly to the instrumentation
185 plan (Figures 2 and 3). The loading point situates at 500 mm (i.e. 10D) above the ground level. The
186 loading was displacement-controlled with a rate of 1 mm/s at the actuator level and terminates at 50
187 mm (i.e. 1D). The measurements of the FBGS, the laser and force transducer were recorded and
188 registered every 0.02 second (i.e., 50 Hz).

189 ***4.2 Horizontal response of the model pile***

190 In Figure 6a, the normal strains measured at each incremental force (every 0.25 kN until 1.75 kN)
191 were plotted versus the pile depth. As the applied horizontal load H increases, the normal strains within
192 the pile increase as well. Under the same H , normal strains first slightly increase with depth, reach to
193 the maximum at the depth of 100 mm and then decrease almost to zero at 425 mm below the ground
194 level. The average value of the tensile and compressive strains was used to determine the bending
195 moments and the used equation was shown in Figure 6b. At the ground level, the moments measured
196 by FBGS (empty circular points) are very close to the moments calculated from H (solid square
197 points), confirming the reliability of the FBGS under flight condition. At the pile end (FBGS #13, z
198 = 425), the bending moments are close to zero. The discrete moments along the depth need to be
199 fitted into continuous so that further calculation can be proceeded. In Haiderali and Madabhushi
200 (2016), the authors compared different curve fitting techniques and found that the cubic and cubic B-
201 splines gave more consistent and accurate P-y curves. In this study, the cubic splines function was
202 used to interpolate the experimental results. According to the beam theory, the shear force V and the
203 transversal distributed loads along the pile P (equal to the soil reaction) can be obtained by solving
204 the first and second derivatives of the moment profiles (i.e. cubic splines), respectively. Due to the
205 lack of the experimental results above the ground surface and below the pile tip, the algorithm of the
206 cubic spline forces the spline approximate the end points (i.e., FBGS #1 and FBGS #13) in a default

207 way, considering the second derivative of the spline to be zero. Such algorithm is normally reasonable
208 for FBGS #1 as the second derivative of the bending moment (i.e., soil reaction) should be
209 theoretically null at the ground level, however, probably incorrect for FBGS #13 because the soil
210 reaction at the pile tip should not be zero. As a result, the first and second derivatives of FBGS #13
211 (i.e. pile depth from 375-425) are not necessarily significant and were not determined. In Figures 6c
212 and 6d, the V and P profiles are presented. For the former, V at the ground level are coherent with H
213 applied by the actuator. Slight difference is due to uncertainties in finding the first derivative
214 accurately as it lacks experimental points above the ground surface. Concerning the P profile, as H
215 increases, the pile rotation centre defined here as the point where the soil reaction is nil, $P = 0$
216 increases from 210 – 275 mm (i.e., 4.2 – 5.5 D) below the ground level.

217 Finding the second-order definite integral of the moment profiles, one may obtain the pile transversal
218 deflection y . This was usually achieved by solving a simultaneous equation that contains two
219 integration constants. Two limit conditions are introduced in this study. The first one is the pile
220 deflection measured by the electric actuator at the pile head. The second is the null pile deflection (y
221 = 0) at the rotation centre, which was determined by finding the depths of the null reaction ($P = 0$),
222 as presented in El Haffar et al. (2019). Figure 7 presents the pile horizontal deflection at different H
223 values. Due to the large embedment depth (i.e., 450 mm or $9D$), pile deflections are close to zero
224 below the rotation centre (e.g., 300 - 450 mm below the ground surface). Presented also are the pile
225 deflections measured by the laser transducer. As H increases, the laser provides extra measurements
226 that are comparable with the measurements provided by the electric actuator.

227 P - y curves are obtained by plotting the pile deflection y versus the soil reaction P at different depths
228 (e.g., the depth of the FBGS). In Figure 8, each curve demonstrates the P - y relationship as H increases
229 from 0.25 – 1.75 kN. P is positive above the pile rotation centre and negative under. The initial soil
230 stiffness, i.e., the initial slope of the P - y curve, increases as the embedment depth increases (from the

231 ground surface to the pile tip). For the soil at a certain depth (e.g., $z = 75$ mm), its stiffness decreases
232 as the horizontal load H increases. In this study, a plateau is reached only for the second level, $z = 25$
233 mm. For deeper levels (e.g. $z = 50 - 225$ mm), the P - y curves show a tendency to be stabilized.
234 However, much more lateral displacement is needed to reach such limit.

235 **5. Conclusions**

236 A model pile was instrumented with two diametrically-opposed optical fibres. The instrumented pile
237 was calibrated at $1\times g$ and then subjected to lateral loading in centrifuge at $100\times g$. The experimental
238 results show that:

- 239 • All the 26 FBGS survived in the $100\times g$ centrifuge test;
- 240 • At the ground level, the moments determined by FBGS are in accordance with the moments
241 calculated from the transversal force;
- 242 • Shear forces at the ground level are slightly larger than the applied transversal forces. Such
243 difference mainly results from the difficulty of the accurate derivation operation at the ground
244 level.
- 245 • The pile local behaviour is characterized: under the effect of the increasing horizontal load, pile
246 rotates at the depth 210 - 275 mm (i.e., $4.2 - 5.5D$) below the ground level. Due to the large
247 embedment depth, the pile deflection below the rotation centre close to zero. The P - y curves at
248 different depths were also determined.

Table 1. Geometric and mechanical characteristics of the pile

Material	Prototype	Model
L (m)	50	0.5
D (m)	5	0.05
d (m)	4.5	0.045
E (GPa)	74 GPa	74 GPa
EI (N.m ²)	7.8×10^{11}	7.8×10^3

Table 2. Characteristics of the Fontainebleau NE34 sand

Sand	C_u (= d_{60}/d_{10})	d_{50} (μm)	$\rho_{d-\text{min}}$ (g/cm^3)	$\rho_{d-\text{max}}$ (g/cm^3)
NE34	1.53	210	1.434	1.746

Acknowledgement

This work benefited from France Energies Marines and State finance managed by the National Research Agency under the Investments for the Future program bearing the reference SOLCYP+ ANR-10-IEED-0006-18. Assistances from the technical staffs of the centrifuge group and discussion with Dr. Thierry Dubreucq are acknowledged.

Reference

- Abadie, C. N., Byrne, B. W., & Houlsby, G. T. (2018). Rigid pile response to cyclic lateral loading: laboratory tests. *Géotechnique*, <https://doi.org/10.1680/jgeot.16.P.325>.
- Barbosa, P., Geduhn, M., Jardine, R. J., & Schroeder, F. C. (2017). Large Scale Offshore Static Pile Tests-Practicality and Benefits. In *Proceeding of 8th International Conference of Offshore Site Investigation Geotechnics*, London, (2): 644-651.
- Baguelin, F. et Jézéquel, J. (1972). Etude expérimentale du comportement de pieux sollicités horizontalement. *Bulletin de Liaison des Ponts et Chaussées*, 62, 129-170.
- Byrne, B. W., McAdam, R. A., Burd, H. J., Houlsby, G. G., Martin, C. M., Beuckelaers, W. J. A. P., ... & Ushev, E. (2017). PISA: New Design Methods for Offshore Wind Turbine Monopiles. In *Proceeding of 8th International Conference of Offshore Site Investigation Geotechnics*, London, (1): 142-161.
- Choo, Y. W., & Kim, D. (2015). Experimental Development of the p-y Relationship for Large-Diameter Offshore Monopiles in Sands: Centrifuge Tests. *Journal of Geotechnical and Geoenvironmental Engineering*, 142(1), 04015058.
- Correia, R., James, S. W., Marshall, A., Heron, C., & Korposh, S. (2016). Interrogation of fibre Bragg gratings through a fibre optic rotary joint on a geotechnical centrifuge. In *Sixth European Workshop on Optical Fibre Sensors (Vol. 9916, p. 99162B)*. International Society for Optics and Photonics.
- Corté, J. F., & Garnier, J. (1986). Une centrifugeuse pour la recherche en géotechnique. *Bulletin de Liaison des Laboratoires des Ponts et Chaussées*, 146, 5-28.
- Cox, W. R., Reese, L. C., & Grubbs, B. R. (1974). Field testing of laterally loaded piles in sand. In *Offshore Technology Conference (OTC 2079)*: 459 - 472.

- Da Silva, T. S., Elshafie, M. Z. E., & Sun, T. (2016). Fibre optic instrumentation and calibration in the geotechnical centrifuge. *Proceeding of the 3rd European Conference on Physical Modelling in Geotechnics*, Nantes, France, 129-135.
- Davisson, M., & Salley, J. (1969). Lateral load tests on drilled piers. *Performance of Deep Foundations*, ASTM STP 444, 68-83.
- Doherty, P., Igoe, D., Murphy, G., Gavin, K., Preston, J., McAvoy, C., Byrne, B. W., Mcadam, R., Burd, H. J., Houlsby, G. T., Martin, C. M. (2015). Field validation of fibre Bragg grating sensors for measuring strain on driven steel piles. *Géotechnique Letters*, 5(2), 74-79.
- El Haffar, I., Blanc, M., & Thorel, L. 2019. Monotonic lateral loading on single piles in sand: parametric centrifuge modelling in eccentricity, saturation and installation mode. *Géotechnique* (submitted).
- France Energies Marines. (2017). SOLlicitations CYcliques des monoPieux d'éoliennes offshore. Accessed on: 2019-04-11. **URL:** <https://solcyp.france-energies-marines.org/>
- Garnier, J. (2001). Modèles physiques en géotechnique-I—Évolution des techniques expérimentales et des domaines d'application. *Revue Française de Géotechnique*, (97), 3-29.
- Garnier, J. (2013). Advances in lateral cyclic pile design: contribution of the SOLCYP project. In *Proceedings of the TC 209 Workshop: 18th ICSMGE—Design for Cyclic Loading: Piles and Other Foundations*, Paris, France, 59-68.
- Georgiadis, M., Anagnostopoulos, C., & Saflekou, S. (1992). Centrifugal testing of laterally loaded piles in sand. *Canadian Geotechnical Journal*, 29(2), 208-216.
- Glisic, B., & Yao, Y. (2012). Fiber optic method for health assessment of pipelines subjected to earthquake-induced ground movement. *Structural Health Monitoring*, 11(6), 696-711.
- Haiderali, A. E., & Madabhushi, G. (2016). Evaluation of curve fitting techniques in deriving p–y curves for laterally loaded piles. *Geotechnical and Geological Engineering*, 34(5), 1453-1473.
- HBM (2019a). Optical Measurement Solutions. Accessed on: 2019-04-09. **URL:** https://www.hbm.com/fileadmin/mediapool/local/.../HBM-FiberSensing_US_web.pdf
- HBM (2019b). X120 adhesive special features. Accessed on: 2019-06-16. **URL:** <https://www.hbm.com/fileadmin/mediapool/hbmdoc/technical/B05001.pdf>
- Hill, K. O., & Meltz, G. (1997). Fiber Bragg grating technology fundamentals and overview. *Journal of Lightwave Technology*, 15(8), 1263-1276.
- Hong, C. Y., Zhang, Y. F., Zhang, Y. W., Borana, L., & Wang, R. F. (2017). New LGFBG-Based structural integrity evaluation method for cement-Grouted soil nails. *International Journal of Geomechanics*, 17(8), 04017026.

- Hussaini, S. K., Indraratna, B., & Vinod, J. S. (2015). Application of optical-fiber Bragg grating sensors in monitoring the rail track deformations. *Geotechnical Testing Journal*, 38(4), 387-396.
- Jardine, R.J., Buckley, R.M., Kontoe, S., Barbosa, P. & Schroeder, F.C. (2018). Behaviour of piles driven in chalk. *Engineering in Chalk*. 33-51
- Kapogianni, E., Sakellariou, M. G., Laue, J., & Springman, S. M. (2010). The use of optical fibre sensors in a geotechnical centrifuge for reinforced slopes. *Proceedings of the 7th International Conference on Physical Modelling in Geotechnics, Zurich, Switzerland*. Vol. 1, 343-348.
- Klinkvort, R. T., & Hededal, O. (2013). Lateral response of monopile supporting an offshore wind turbine. *Proceedings of the ICE-Geotechnical Engineering*, 166(2), 147-158.
- Klinkvort, R. T., & Hededal, O. (2014). Effect of load eccentricity and stress level on monopile support for offshore wind turbines. *Canadian Geotechnical Journal*, 51(9), 966-974.
- Klinkvort, R. T., Britta Bienen B., Fan, S., Black, J., Bayton, S., Thorel, L., Blanc, M., Madabhushi, G., Haigh, S., Broad, T., Zania, V., Askarinejad, A., Li, Q., Kim, D. S., Park, S. (2019). Centrifuge modelling considerations of laterally loaded monopiles in sand. *Géotechnique* (submitted).
- Klinkvort, R. T., Hededal, O., & Springman, S. M. (2013). Scaling issues in centrifuge modelling of monopiles. *International Journal of Physical Modelling in Geotechnics*, 13(2), 38-49.
- Koukoura, C., Natarajan, A., & Vesth, A. (2015). Identification of support structure damping of a full scale offshore wind turbine in normal operation. *Renewable Energy*, 81, 882-895.
- Kreuzer, M. (2006). Strain measurement with fiber Bragg grating sensors. HBM, Darmstadt, S2338-1.0 e.
- LeBlanc, C., Houlsby, G. T., & Byrne, B. W. (2010). Response of stiff piles in sand to long-term cyclic lateral loading. *Géotechnique*, 60(2), 79-90.
- Lee, W., Lee, W. J., Lee, S. B., & Salgado, R. (2004). Measurement of pile load transfer using the Fiber Bragg Grating sensor system. *Canadian Geotechnical Journal*, 41(6), 1222-1232.
- Li, Z., Haigh, S. K., & Bolton, M. D. (2010). Centrifuge modelling of mono-pile under cyclic lateral loads. *Proceedings of the 7th International Conference on Physical Modelling in Geotechnics, Zurich, Switzerland*, 965–970
- Little, R. L., & Briaud, J. L. (1988). Full scale cyclic lateral load tests on six single piles in sand. *Miscellaneous Paper GL-88-27, Geotechnical Division, Texas A&M University, College Station, Texas 77843*
- McAdam, R., Byrne, B.W., Houlsby, G., Beuckelaers, W.J.A.P., Burd, H., Gavin, K., Igoe, D., Jardine, R., Martin, C., Muir Wood, A. & Potts, D. (2018). Monotonic laterally loaded pile testing in a dense marine sand at Dunkirk. *Géotechnique*.

- Ng, C.W.W., Shi, C., Gunawan, A., Laloui, L., and Liu, H.L. 2015. Centrifuge modelling of heating effects on energy pile performance in saturated sand. *Canadian Geotechnical Journal* 52(8): 1045-1057.
- Ni, P., Moore, I.D., and Take, W.A. 2018. Distributed fibre optic sensing of strains on buried full-scale PVC pipelines crossing a normal fault. *Géotechnique* 68(1): 1-17.
- Park, S., Park, T., & Han, K. (2011). Real-time monitoring of composite wind turbine blades using fiber Bragg grating sensors. *Advanced Composite Materials*, 20(1), 39-51.
- Puech, A. and Garnier, J. (2017). *Design of piles under cyclic loading: SOLCYP recommendations*. Wiley-ISTE, 454 pages.
- Reese, L. C., Cox, W. R., & Koop, F. D. (1974). Analysis of laterally loaded piles in sand. In *Offshore Technology Conference (OTC 2080)*, 473 - 483.
- Rosquoet, F., Thorel, L., Garnier, J., & Canepa, Y. (2007). Lateral cyclic loading of sand-installed piles. *Soils and Foundations*, 47(5), 821-832.
- Simpson, B., Hoult, N. A., & Moore, I. D. (2015). Distributed sensing of circumferential strain using fiber optics during full-scale buried pipe experiments. *Journal of Pipeline Systems Engineering and Practice*, 6(4), 04015002.
- Saiyar, M., Ni, P., Take, W.A., and Moore, I.D. 2016. Response of pipelines of differing flexural stiffness to normal faulting. *Géotechnique* 66(4): 275-286.
- Ting, J. M. (1987). Full-scale cyclic dynamic lateral pile responses. *Journal of Geotechnical Engineering*, 113(1), 30-45.
- Truong, P., Lehane, B. M., Zania, V., & Klinkvort, R. T. (2018). Empirical approach based on centrifuge testing for cyclic deformations of laterally loaded piles in sand. *Géotechnique*, 69(2), 133-145.
- Verdure, L., Garnier, J., & Levacher, D. (2003). Lateral cyclic loading of single piles in sand. *International Journal of Physical Modelling in Geotechnics*, 3(3), 17-28.
- Weng, X., Zhao, Y., Lou, Y., & Zhan, J. (2016). Application of Fiber Bragg Grating Strain Sensors to a Centrifuge Model of a Jacked Pile in Collapsible Loess. *Geotechnical Testing Journal*, 39(3), 362-370.
- Wind Europe. (2017). 'The European onshore wind industry - key trends and statistics 2016'. Accessed on: 2016-07-03.
- Zhu, H. H., Yin, J. H., Jin, W., & Zhou, W. H. (2007). Soil nail monitoring using Fiber Bragg Grating sensors during pullout tests. *The Joint 60th Canadian Geotechnical and 8th IAH-CNC Conferences*. Ottawa, Canada, 821-828.

Zhu, H. H., Yin, J. H., Yeung, A. T., & Jin, W. (2011). Field pullout testing and performance evaluation of GFRP soil nails. *Journal of Geotechnical and Geoenvironmental Engineering*, 137(7), 633-64.

FIGURE CAPTIONS

Figure 1 Working principle of the Fibre Bragg Grating sensors

Figure 2 Instrumentation of the model pile

Figure 3 Experimental set-up for the calibration of the instrumented pile

Figure 4 Measurements of the FBG sensors for the calibration test

Figure 5 Schematic drawing of the transversal loading system in the centrifuge

Figure 6 Profile of (a) the measured strains, (b) the bending moment, (c) the shear force and (d) the soil reaction (i.e., the distributed load)

Figure 7 Deflection of the pile below and above the ground level

Figure 8 Soil reaction (P) versus the normalized pile deflection (y/D)

FIGURE CAPTIONS

Figure 1 Working principle of the Fibre Bragg Grating sensors

Figure 2 Instrumentation of the model pile

Figure 3 Experimental set-up for the calibration of the instrumented pile

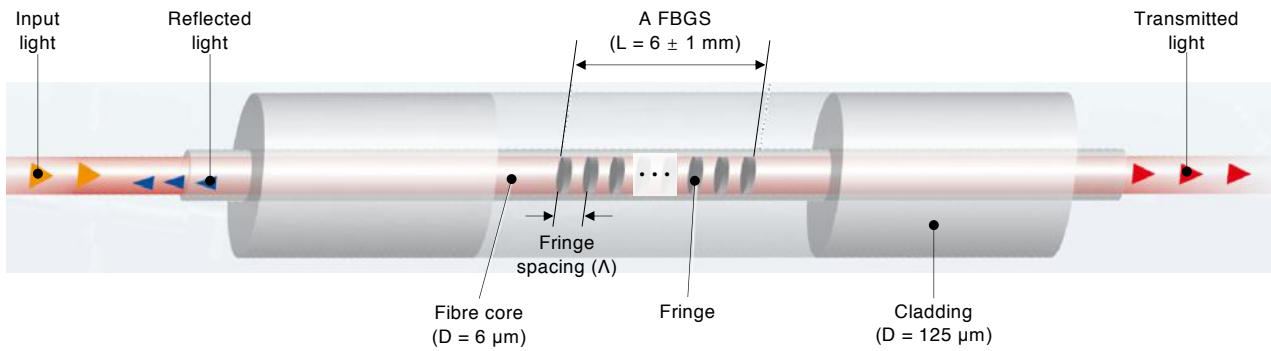
Figure 4 Measurements of the FBG sensors for the calibration test

Figure 5 Schematic drawing of the transversal loading system in the centrifuge

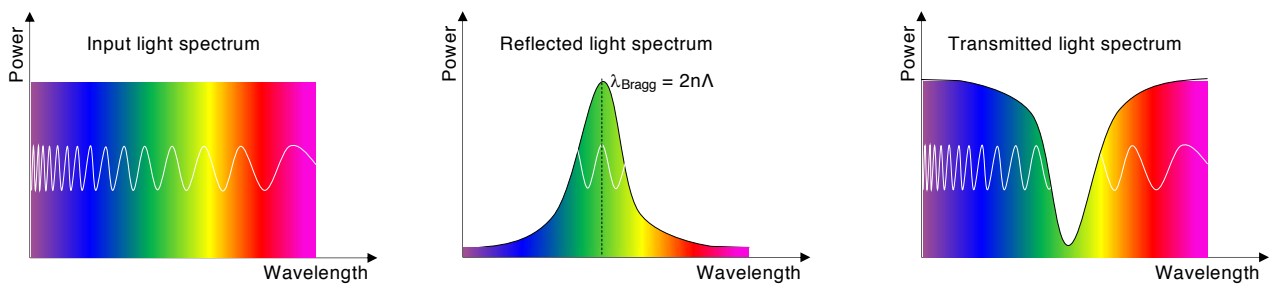
Figure 6 Profile of (a) the measured strains, (b) the bending moment, (c) the shear force and (d) the soil reaction (i.e., the distributed load)

Figure 7 Deflection of the pile below and above the ground level

Figure 8 Soil reaction (P) versus the normalized pile deflection (y/D)



(a) Composition of the fibre (after HBM, 2019a)



(b) Wave propagation in the Bragg optical fibre

Figure 1 Working principle of the Fibre Bragg Grating sensors

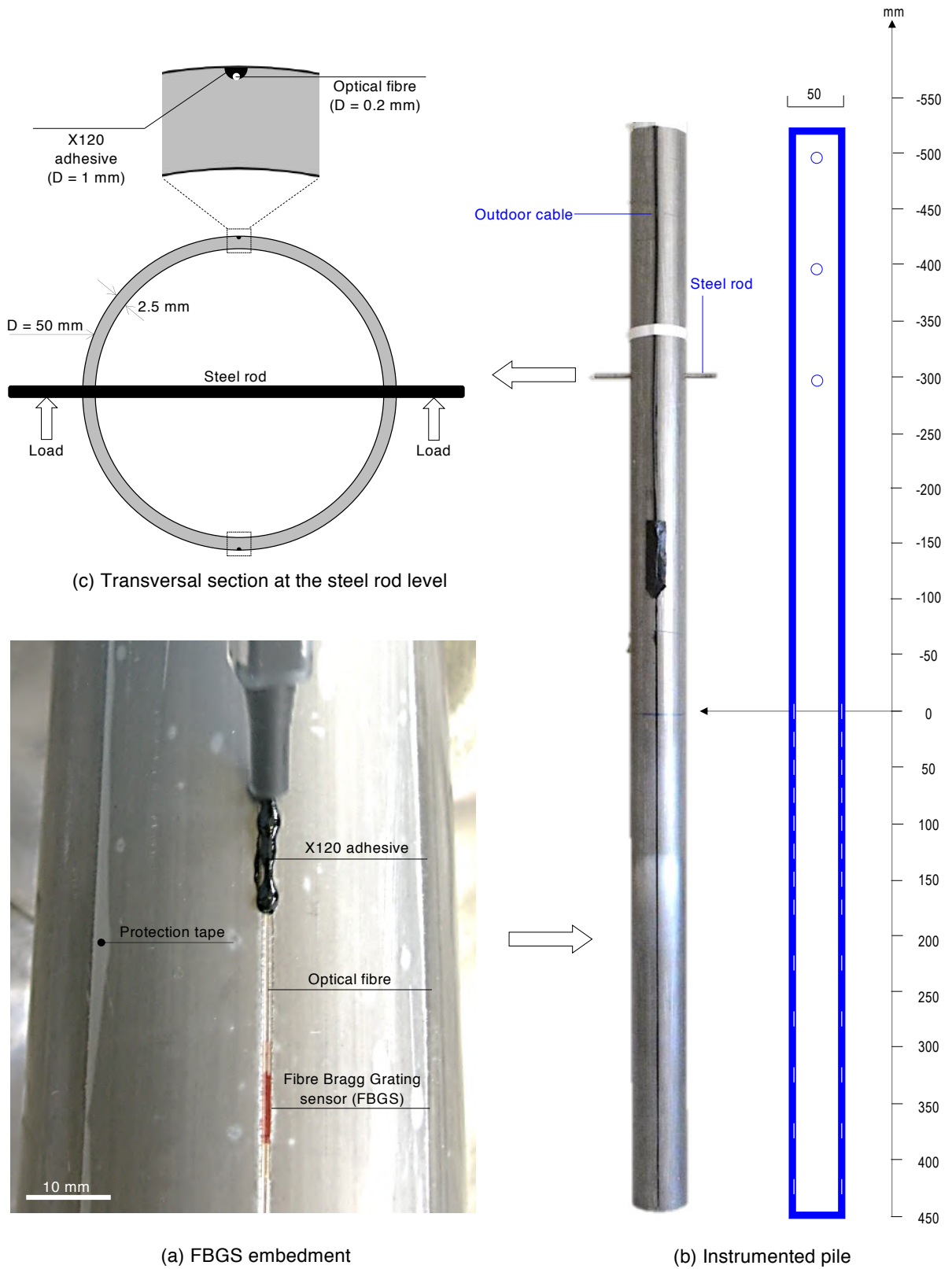
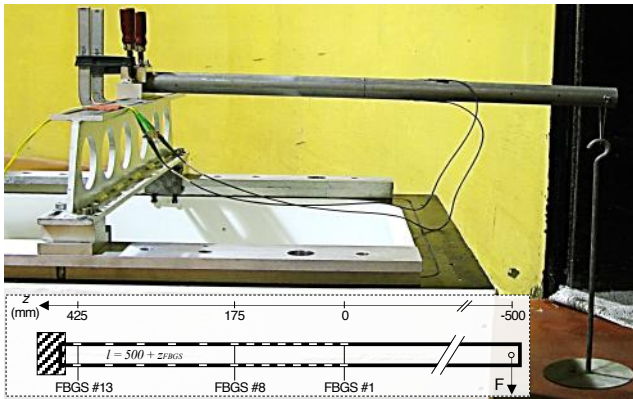
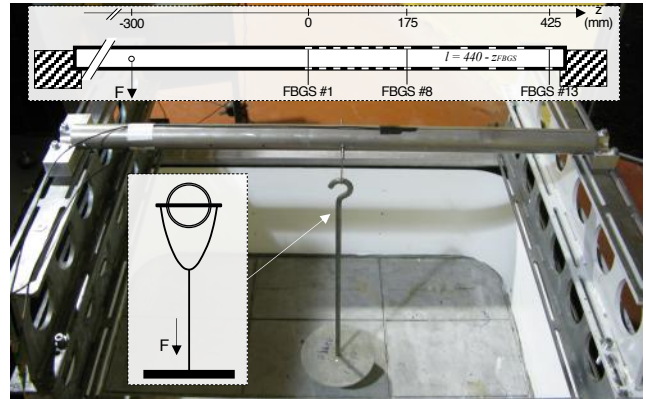


Figure 2 Instrumentation of the model pile

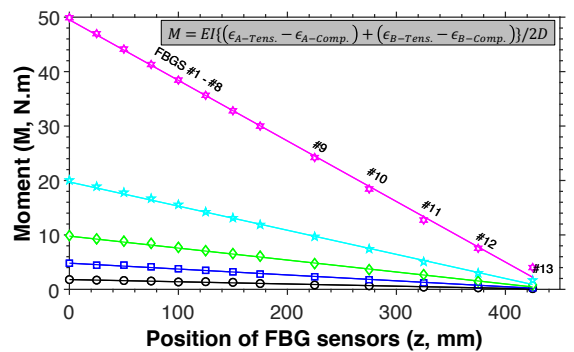
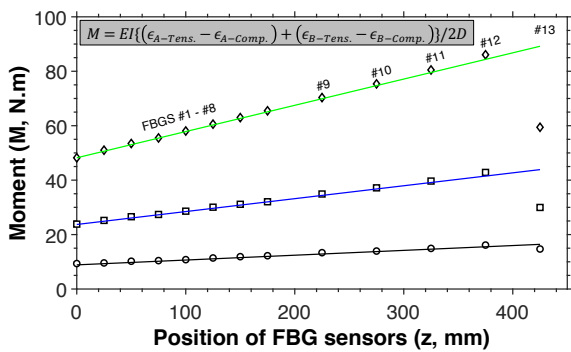
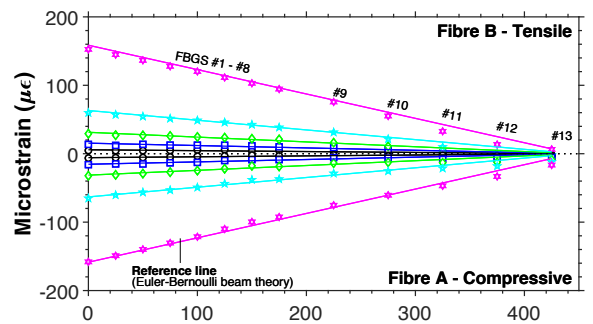
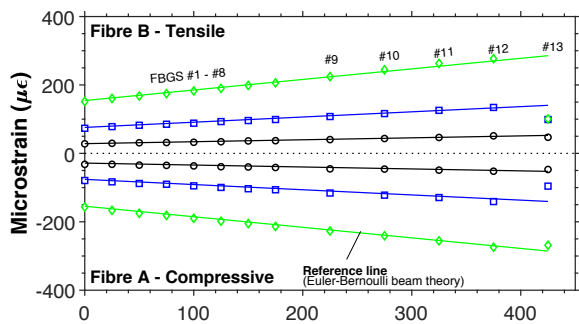
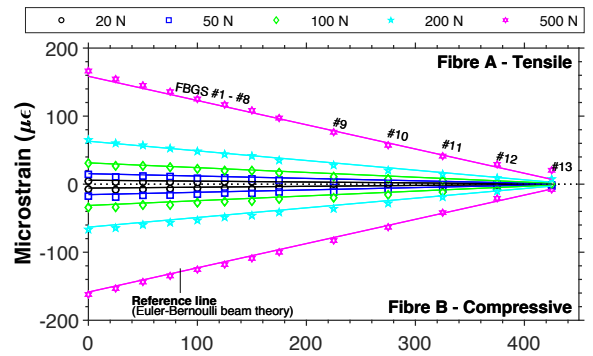
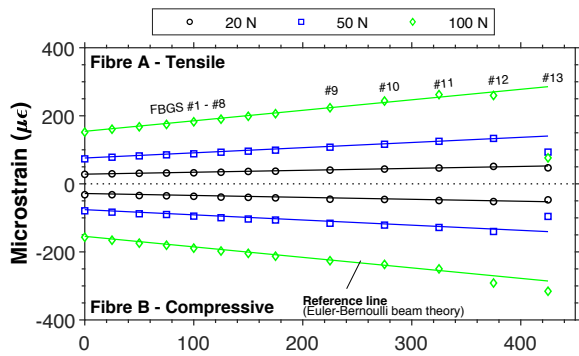


(a) Cantilever beam configuration



(b) Simply supported beam configuration

Figure 3 Experimental set-up for the calibration of the instrumented pile



(a) Cantilever beam

(b) Simply supported beam

Figure 4 Measurements of the FBG sensors for the calibration test

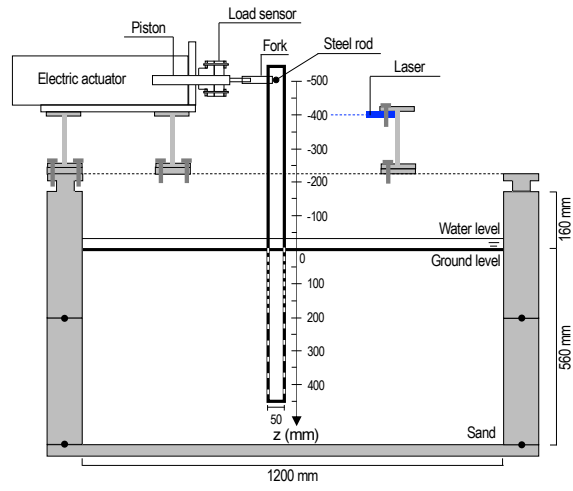


Figure 5 Schematic drawing of the transversal loading system in the centrifuge

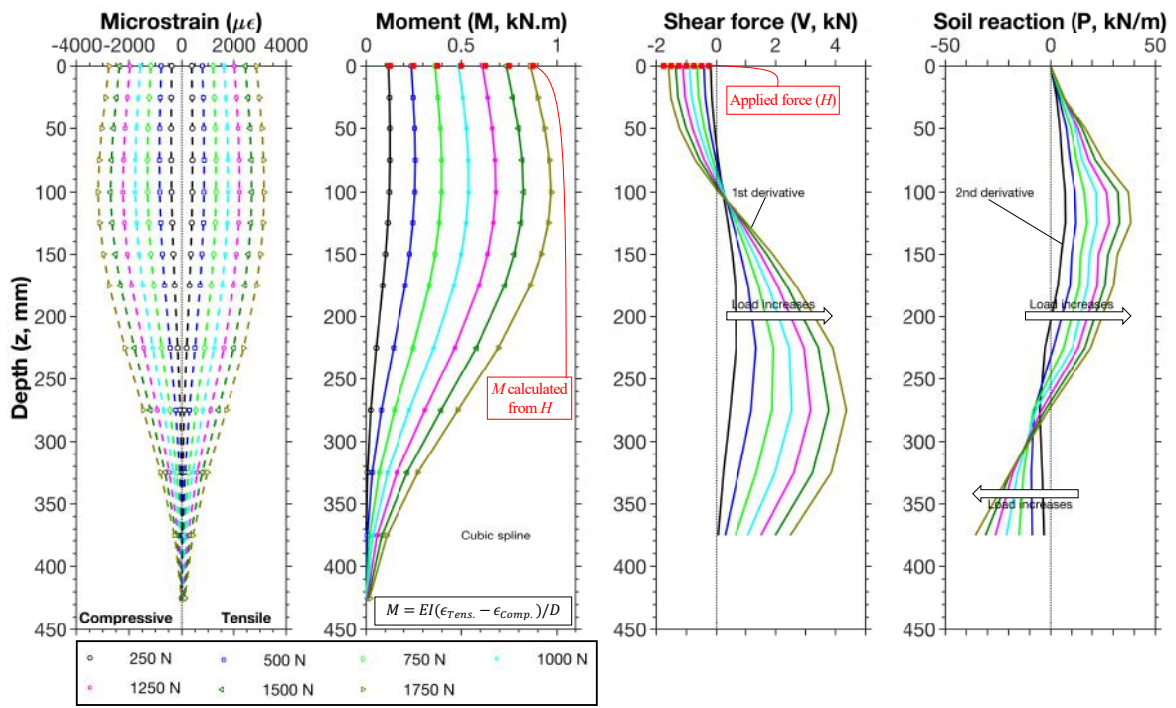


Figure 6 Profile of (a) the measured strains, (b) the bending moment, (c) the shear force and (d) the soil reaction (i.e., the distributed load)

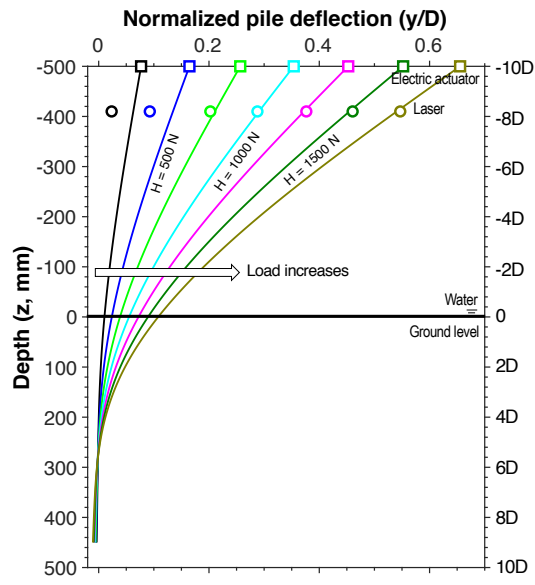


Figure 7 Deflection of the pile below and above the ground level

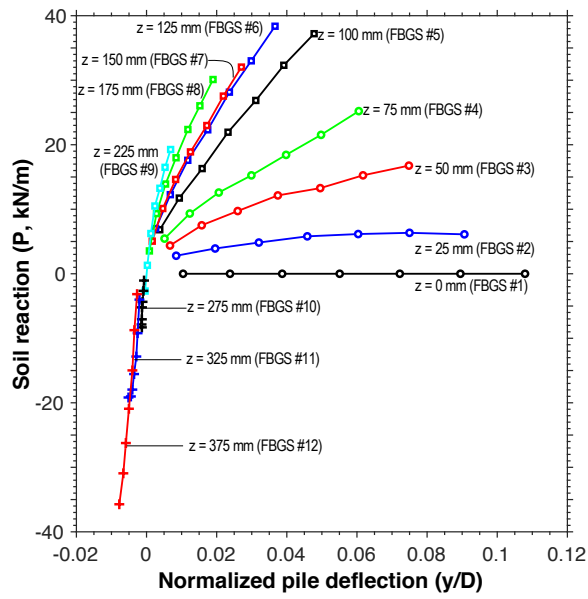


Figure 8 Soil reaction (P) versus the normalized pile deflection (y/D)